PROC. INST. ACOUSTICS VOL 7 PT 3 1985

SEAFLOOR CLASSIFICATION USING SONAR ECHO STATISTICS

Timothy K. Stanton

University of Wisconsin-Madison, U.S.A.

ABSTRACT

Sonars are used to remotely map and classify the seafloor. Microrelief features such as rocks, nodules, and sand ripples are of great interest in the applications of the propagation of communication signals, mining, and geological studies. These features, however, are not resolvable by standard sonars. We can learn about the microrelief of the seafloor from the amplitude fluctuations they cause in sonar echoes as the sonar is towed over a rough area. Fluctuations are caused by the interferences between the individual protuberances of the microrelief. We describe the fluctuations with the Rice PDF (probability density function). We combine Eckart's acoustic scattering theory with Rician statistics to describe echo fluctuations of sonar echoes from the seafloor in terms of the rms roughness and the correlation area. (The area is defined as the product of the x and y correlation distances along the seafloor). With our formulation we perform both inverse and forward calculations. Inverse: We use echo data to estimate the microrelief. Forward: From microrelief information we predict fluctuations for several sonars and reliefs.

INTRODUCTION

To directly measure the microrelief of the seafloor, one needs ultra-high resolution sonars; i.e. ultra narrow beams and very short ping durations. Figure 1 illustrates this ideal requirement alongside what is commonly done. With the ideal system, the seafloor microrelief could be resolved and there would be more certainty in the classification of the property than if systems of lower resolution were used. These high resolution systems would require a physically large aperture or a parametric source to produce such narrow beams. A broadband or high frequency source is required for short pings. Some form of a multibeam system is required for high coverage.

In the standard systems such as downward looking 3.5 kHz and 12 kHz sonars the microrelief is not resolved and the sonar echo is a composite of the unresolved returns. The echoes from the individual rocks, nodules, or ripples will contribute to the total received echo. Because of the different phases of the individual echoes, they will interfere with each other. As a result, as a sonar is towed over the seafloor, the received (total) echo will fluctuate from ping to ping.

We use the nature of the fluctuations of the echo from the seafloor to estimate the microrelief. We begin by examining Clay and Medwin's generalized version [1] of Eckart's acoustic scattering theory [2]. We combine it with Rice's envelope statistics [3] to derive an equation describing the echo amplitude fluctuations in terms of the rms roughness and correlation area. We use the formulation to estimate the microrelief from sonar echo data from several areas in the North Atlantic. Predictions of echo fluctuations are also made using the acoustically measured microrelief for several sonars and sediment types.

THEORY AND EXPERIMENT

Because of the shortness of this paper, many steps in the following derivations are left out. For the complete derivations, see references [7] and [12].

Moments.

Statistical descriptions of sonar signals reflected at a rough interface are often expressed in terms of the moments of the signal. The first moment is the coherent component. It is the average or "stack" of repeated transmissions when the rough surface is moved between each transmission. If the surface is planar or smooth, all transmissions are the same and the average stacked signal is identical to a single transmission. If the surface is very rough, the echoes differ and the average or stacked signal tends to zero. Eckart used the Helmholtz integral and Kirchhoff approximation to calculate the coherent reflection for a rough surface having a normal or Gaussian PDF [2]. The coherently reflected signal is

First moment:

$$\langle p \rangle = \mathcal{R}_{COH} \frac{B}{2R_1} \tag{1}$$

where $\mathcal{R}_{COH} = Re^{-2k^2\sigma^2\cos^2\theta}$

and R is the Rayleigh reflection coefficient, k is the wavenumber, σ is the rms roughness, θ is the angle of incidence, and B is a source constant. One can use measurements of $\mathcal{R}_{COH}$ and Eq. (1) as a function of frequency to estimate σ. For small $k\sigma\cos\theta$ the echo is mostly reflected. As $k\sigma\cos\theta$ increases, scattering dominates the echo and the coherent component of the echo is diminished exponentially.

The second moment of the signal about the mean signal depends on the roughness and the spatial correlation function of the rough surface. Computations of the mean squared signal are much more complicated than computations of the mean stacked signal. We give the results of a computation that uses Eckart's procedure with an extension including a spherical wave front or Fresnel correction. Chapter 10 and appendix A10 of Clay and Medwin give a derivation [1]. At vertical incidence with the source and receiver at the same positions, the mean square scattered signal is, (Eqs. (A10.5.20), (A10.5.21), and (A10.5.10))

Second moment:

$$\langle p^2 \rangle = \frac{k^2B^2R^2XY}{8\pi R_1^4} \int_{-\infty}^{\infty}\int \mathcal{G}\mathcal{W}\, d\xi d\eta \tag{2}$$

where

$$\mathcal{G} = \exp\left[-(a_\xi \xi^2 + a_\eta \eta^2)\right], \quad \mathcal{W} = \exp\left[-4k^2\sigma^2(1-C(\xi,\eta))\right]$$

$$a_\xi = \frac{X^2}{2x_f^4} + \frac{1}{2X^2} \quad , \qquad a_\eta = \frac{Y^2}{2y_f^4} + \frac{1}{Y^2}$$

$$x_f^{-2} = \frac{k}{R_1} \quad , \qquad y_f^{-2} = \frac{k}{R_1}$$

$$X = R_1 \Delta\chi \quad , \qquad Y = R_1 \Delta\phi$$

where we let $\theta_1 = \theta_2 = 0$, and $R_1 = R_2$ in the Clay and Medwin equations. And, where R_1 is the depth, B is a source constant, $\Delta\chi$ and $\Delta\phi$ are sonar beam half widths, and $C(\xi,\eta)$ is a spatial correlation function. Since Clay and Medwin wrote their book, experiments have shown Helmholtz-Kirchhoff solution to be very inaccurate at shallow grazing angles [4]. Experiments have shown the Helmholtz-Kirchhoff solution to be accurate near vertical incidence [5,6]. Since our application is near vertical incidence, we use Eq. (2) for our computations. Clay and Medwin give an evaluation of Eq. (2) for second-order polynomial approximations to $C(\xi,\eta)$ that is valid for a wide range of $k\sigma$. For $4k^2\sigma^2 << 1$ we expand the exponential in W and write Eq. (2) as

$$\langle p^2 \rangle \approx \frac{k^2 B^2 R^2 XY}{8\pi R_1^4} \left[e^{-4k^2\sigma^2} \int_{-\infty}^{\infty}\int \mathscr{D} d\xi d\eta + 4k^2\sigma^2 e^{-4k^2\sigma^2} \int_{-\infty}^{\infty}\int \mathscr{D} C(\xi,\eta) d\xi d\eta \right] \quad (3)$$

The integral in the first term is $\pi/(a_\xi a_\eta)^{1/2}$ giving

$$\text{first term} = \frac{k^2 B^2 R^2 XY}{8R_1^4} \frac{e^{-4k^2\sigma^2}}{(a_\xi a_\eta)^{1/2}} \quad (4)$$

$$= \langle p \rangle^2$$

This is the image solution and is the square of the coherently reflected component (Eq. (1). The second term is the mean square scattered signal $\langle s^2 \rangle$:

$$\langle s^2 \rangle = \frac{k^2 B^2 R^2 XY}{8\pi R_1^4} 4k^2\sigma^2 e^{-4k^2\sigma^2} \int_{-\infty}^{\infty}\int \mathscr{D} C(\xi,\eta) d\xi d\eta \quad (5)$$

Thus we write

$$\langle p^2 \rangle = \langle p \rangle^2 + \langle s^2 \rangle \quad (6)$$

Where $\langle p \rangle^2$ is the square of the first moment and $\langle s^2 \rangle$ is the mean squared scattered signal.

Rice PDF.

In electrical signal theory, Rice derived an expression for the PDF of the

envelope of a sine wave and noise [3]. The PDF of a sine wave alone is the Delta function. The Rayleigh PDF describes the noise alone. We make an analogy between the electrical case and the acoustical one. The coherent component $\langle p \rangle$ has a Delta function PDF and corresponds to the sine wave. The random scattered component s has a Rayleigh PDF and corresponds to the noise. The envelope of the total echo then has a Rice PDF.

We define γ as

$$\gamma = \frac{\text{coherently reflected echo energy}}{\text{incoherently scattered echo energy}} = \frac{\langle p \rangle^2}{\langle s^2 \rangle} \tag{7}$$

In the electrical analogy, γ would be the signal-to-noise ratio. We now write the Rice PDF to describe the echo amplitude $e = (pp^*)^{1/2}$ from the seafloor as [7]

$$w(e) = \frac{2(1+\gamma)e}{\langle e^2 \rangle} \exp\left(- \frac{(1+\gamma)e^2 + \gamma\langle e^2 \rangle}{\langle e^2 \rangle} \right) I_0(q') \tag{8}$$

$$\text{where } q' = \frac{2e[\gamma(1+\gamma)]^{1/2}}{\langle e^2 \rangle^{1/2}}$$

Figure 2 illustrates the Rice PDF for a range of values of γ. For $\gamma = 0$, the Rice PDF is the Rayleigh PDF. This occurs, as Eq. (7) shows, when the echo is totally dominated by scattering. The surface is so rough that there is no coherent return and there is much fluctuation in the echo. When the surface becomes very smooth, the coherent component of the echo dominates and the PDF tends to the Gaussian. In this case the echo fluctuates very little. For intermediate roughnesses, the PDF takes on intermediate curves. The Rice PDF varies smoothly between the extremes.

Using Eqs. (4)-(7), γ is written in terms of the acoustic scattering process:

$$\gamma^{-1} = \frac{4ak^2\sigma^2}{\pi} \int_{-\infty}^{\infty}\int \mathscr{G}(\xi,\eta) C(\xi,\eta)\, d\xi d\eta \qquad \text{for } 4k^2\sigma^2 << 1 \tag{9}$$

$$a = (a_\xi a_y)^{1/2}$$

This equation is crucial to the description of the echoes from the sea floor. It has been shown that in many experiments, it can be simplified into a more pratical form [7,12]. To summarize those discussions, in many typical experiments, the correlation function $C(\xi,\eta)$ will dominate. We consider "typical" to be a 3.5 kHz downward-looking sonar with a 30° beamwidth and a floor consisting of current generated ripples or small rocks. We then can write Eq. (9) as

$$\gamma^{-1} = \left(\frac{1}{2\pi}\right) k^4 \chi^2 \sigma^2 I_C \tag{10}$$

where

$$I_C = \iint C(\xi,\eta)\,d\xi\,dy$$

And $\chi = \frac{2X}{R}$ = full beamwidth (between e^{-1} points in radians)

Equation (10) is a very important equation in describing the echo fluctuations from the rough seafloor. What is especially important is that the fluctuations are described in terms of the integral of the correlation function, not the correlation function itself. It is very difficult to know the exact correlation function from point to point along the seafloor. Any uncertainties in estimating it would tend to average to zero in the integration.

We will further evaluate the integral of the correlation function. However, in general, the essential information to understanding fluctuations from the seafloor is the product $\sigma^2 I_C$. It can be extracted from fluctuation data to classify the sea floor or, once known, be used to predict echo fluctuations under a variety of sonar geometries.

To evaluate Eq. (10), we use a convenient correlation function of the floor. It is illustrated in Fig. 3 along with a drawing of a floor with current generated ripples as the dominant roughness. Using the correlation function to evaluate I_C in Eq. (10) we find γ^{-1} to be

$$\gamma^{-1} = \left(\frac{1}{3\pi}\right) k^4 \sigma^2 \chi^2 \ell_x \ell_y \qquad (11)$$

Equation (11) is an algebraic equation that describes echo fluctuations from the seafloor in the small roughness case. The term γ that determines the shape of the PDF of the echo envelope is expressed in terms of the wavenumber, beamwidth, rms roughness and what we call the correlation area $\ell_x \ell_y$ of the floor.

Figure 4 illustrates typical echo PDF data collected on the continental shelf near Cape Hatteras, North Carolina. We employed a 3.5 kHz downward looking sonar. The most striking difference between the two PDFs is the difference in shapes (and subsequently values of γ). The PDF of the bottom in region 1 is sharply peaked and Gaussian-like. The PDF of the bottom in region 2 is broad with a shape resembling the Rayleigh distribution. The values of γ in the two cases are approximately 240 and 1, respectively. These values also reflect the Gaussian-like and Rayleigh-like resemblances. As previously discussed, curves with high values of γ indicate a high signal-to-noise ratio of coherent-reflection-to-incoherent-scattering. Since the PDF is so sharply peaked the bottom appears to be quite smooth with a very small degree of roughness. In region 2 where the value of γ is relatively low, there is a mixture of coherence and incoherence in the echo. Since there is little difference between curves with $\gamma = 0$ and $\gamma = 1$ (see Fig. 2) and the fitting of the curve to the PDF in region 2 was relatively arbitrary then its value could easily be equal to 0. In that case the echo from the bottom is totally randomly scattered. In either case, the bottom in region 2 is rougher than in region 1.

Ground truth is ultimately necessary to test the accuracy of our analysis of this data. Since that is not available, we can make a rough test of the data by

first assuming that the floor consisted of current generated ripples. This is a reasonable assumption for this part of the continental shelf. Clay and Leong [8] used empirical data from Heezen and Hollister [9] to express the correlation distance of the ripples in terms of their rms roughness. We have used their expression to rewrite our expression for Υ:

Ripples:

$$\Upsilon^{-1} = \frac{300}{\pi} \chi^2 \alpha k^4 \sigma^{4.5} \qquad (\sigma \text{ in meters}) \qquad (12)$$

where $\alpha = \ell_y/\ell_x$ and can range from 1 to 5.

Equation (12) shows that for current generated ripples, Υ, which determines the shape of the echo PDF, is expressed in terms of the sonar beamwidth, the acoustic wavenumber, a constant relating the x and y correlation distances, and the rms roughness. The 4.5 exponent to σ shows how sensitive the echo PDF is to the roughness. A slight change in roughness will cause a great change in the shape of the PDF.

For our 3.5 kHz sonar, $k = 14.7\ m^{-1}$ and the beamwidth was 40° (χ = 68° = 1.2 radians). With α being in the range 1 to 5, the rms roughness σ is in the range 0.8 cm to 1.2 cm in region 1. The range of σ reflects the range of α. Since in region 2, Υ may be equal to zero and the roughness may tend to be undeterminably large, we can only estimate a lower bound in the roughness there. Using $\Upsilon = 1$ we calculate the lower bound of σ to be in the range 2.7 to 3.9 cm. Again, the range in σ reflects the range in α. The results in both regions are consistent with the relief observed in that area.

In this section, we have shown that with coherent or "stacked" data one can determine the rms roughness of the seafloor using Eckart's equation (Eq. (1)). From echo fluctuation data such as the PDFs shown one can determine the product $\sigma^2 \ell_x \ell_y$ where $\ell_x \ell_y$ is the "correlation area" of the floor from Eq. (11). Using the value of σ from the Eckart approach we can then determine the correlation area alone. These two properties help classify the seafloor. This can be important in discriminating between different types of seafloors. For example, an area with only ripples may have the same rms roughness as an area that contains rocks or nodules. However, the correlation areas may be drastically different. This difference would be indicated by the difference in shapes of the PDFs of the echo envelopes from the two areas.

Multifrequency and Coherence functions.

The experiment just described illustrated echo PDFs for two different roughnesses. For an rms roughness of about 1 cm, the PDF was sharply peaked and Gaussian-like. In the other case, the lower bound in roughness was about 3 cm and the PDF was Rayleigh-like. Thus while the roughnesses potentially were not very different, the PDFs were quite different. While the data from this single frequency system were informative, Eqs. (11) and (12) as well as this data show that the PDF is strongly dependent upon frequency and rms roughness. If there is a small change in rms roughness, a large change in the PDF will occur, thus the dynamic range of measurement of roughness is quite limited. Use of a broadband acoustic source can provide the range in frequencies necessary in adequately classifying the range in relief of the seafloor.

In this section, we describe a series of measurements performed by Dunsiger et al. [10] who used a broadband boomer source [11]. In the frequency range of about 1 kHz to 10 kHz they performed their experiments on the Grand Banks of Newfoundland over areas of silt, sand, till and clay. We use their data to estimate the product $\sigma^2 I_C$ for two different types of sediment. We implement the estimates of $\sigma^2 I_C$ from Dunsiger's data to predict PDFs for other sonars, not necessarily their boomer.

Dunsiger measured, among other things, "reflection coherence functions." Their reflection coherence function CF_R was expressed as

$$CF_R(f) = \frac{\text{Power spectrum of aligned and stacked echoes}}{\text{Average power spectrum of individual echoes}}$$

$$= \frac{\langle p \rangle^2}{\langle p^2 \rangle} \qquad (13)$$

The numerator of CF_R was calculated by first carefully aligning the echoes so as to remove phase shifts due to depth changes. The echoes were then stacked and a power spectrum was calculated from the result. CF_R represents the fraction of echo power that is "reflected" or coherent over the entire profile area. Note that in the notation of Dunsiger et al., CF_R was "γ_R." However, to avoid confusion in this paper we replace their "γ_R" with CF_R.
Using Eqs. (6) and (7) we can write $CF_R(f)$ in terms of γ [12]:

$$CF_R(f) = \frac{1}{1+\gamma^{-1}} \qquad (14)$$

The echo envelope PDF and measured coherence function are then related by this simple equation.

The beamwidth of the boomer signal was a function of frequency. To account for this we used an empirical equation given by Dunsiger et al. that expressed the beamwidth in terms of the acoustic frequency to allow us to rewrite Eq. (10):

Boomer:

$$\gamma^{-1} = 1.26\times10^{10} c^{-4} (\text{Hz})^2 f^2 \sigma^2 I_C \qquad (15)$$

Figure 5 shows the measured CF_R for areas of clay and silt. Superimposed on the data are plots of CF_R from Eq. (14) using the adapted γ from Eq. (15). In each graph there is good agreement between experiment and theory for frequencies above about 6 kHz. Below 6 kHz there is a natural departure. This arises from the fact that the Eckart theory used to derive γ is a CW one and the boomer transmits a transient. As previously discussed, the boomer source has a frequency dependent beampattern. The beams are narrow at high acoustic frequencies and wide at low frequencies. Also because of the high resolution spectral analysis, there is an effective pulse elongation or ringing. Between

the combination of those two effects there is much overlap between all returns from the insonified portion of the floor at high frequencies. At these frequencies we then effectively have a CW signal so that the Eckart CW theory applies. Conversely at the low frequencies there is not overlap and the theory does not apply. Figure 6 summarizes the results in Fig. 5. Listed are values of the important roughness property measured, the $\sigma^2 I_C$ product. This product was taken directly from the fit of Eq. (14) and using Eq. (15) to the measured data. It is this product that will later be used to predict echo amplitude PDFs. Also given is the rms roughness σ of each sediment as measured by photographs at several sites.

PDF Predictions.

Figure 6 gives a table of all the critical input necessary to predict the fading patterns. Figures 7 and 8 present predictions of various echo envelope PDFs using $\sigma^2 I_C$ microrelief data from Fig. 6 as input into Eqs. (10) and (8). The "smooth" and "rough" clay correspond to the upper and lower curves from Fig. 5. The PDFs represent echoes from downward looking sonars (not necessarily the boomer) for various frequencies, beamwidth, and two types of sediments. Since the "smooth" clay and silt had such similar values of $\sigma^2 I_C$ ($3.1 \times 10^{-6} m^4$ and $3.0 \times 10^{-6} m^4$, respectively), the $3.0 \times 10^{-6} m^4$ value was chosen to calculate the PDFs for both of them. The major assumptions in the calculations are that (1) the ping is sufficiently long so that echoes from all portions of the insonified area sufficiently overlap and (2) the echo fluctuations are solely due to roughness of the water/bottom interface.

Figure 7 shows that the higher the frequency and/or the rougher the terrain, the more the echo will fluctuate or fade. The PDFs are Rayleigh-like for the high frequency (12 kHz) and tending toward a narrow Gaussian for the low frequency (3.5 kHz). The "rough" clay in Fig. 7b produces greater fluctuations than "smooth" clay and silt in Fig. 7a as one would expect. This is consistent with Fig. 5 where the coherence function for "rough" clay decreases quicker with increasing frequency than for the other sediments.

Figure 8 shows that the narrower the beam, the narrower the PDF, therefore the less the signal will fluctuate. This is indicative of the fact that less of the rough surface contributes to the echo for the narrow beam. As Eq. (1) shows, the coherent or reflected component of the echo is independent of beamwidth. Therefore the narrower the beam, the ratio of scattered energy to reflected energy decreases and hence so do the fluctuations.

CONCLUSIONS

Very high resolution is required to adequately classify the seafloor using sonars. When such resolution is not available, we employ indirect or "inverse" techniques. We have described in this paper methods to estimate properties of the seafloor from the statistical nature of the echo.

Resolution and echo fluctuations are interrelated. When objects or surfaces are adequately resolved, the only fluctuations as the sonar is moved are due to variations in local reflectivities. As the resolution is decreased, there is interference between the unresolved features and the echo fluctuates more. From models of the seafloor, we have made forward calculations to predict the

fluctuations. From echo fluctuation data and other independent measurements we have used our insight gained from the forward calculations to estimate the type of seafloor present.

When using sonars to remotely classify the seafloor, there is a tradeoff between 1) high resolution systems and direct analytical techniques and 2) lower resolution systems and indirect analytical techniques. High resolution sonars give a direct mapping of the environment. However, because of low volume coverage in a high resolution system, multibeams are usually required. As a result, such systems produce much data at a high rate. The engineering challenge is then to process and display the data in a useful form. It is crucial that the display produces meaningful images in real time so that sampling decisions can be made. The data should be presented so that quantitative information is obtainable. With low resolution systems high volume coverage is obtained with a single beam. However, interpretation of the data may be involved and indirect. Therefore when choosing a sonar to remotely classify the seafloor, the interrelationship between resolution and echo fluctuations and the resultant tradeoffs must be studied carefully.

ACKNOWLEDGEMENTS

I am grateful to Professor C.S. Clay of the Department of Geology and Geophysics, University of Wisconsin-Madison, U.S.A. for his invaluable suggestions and the U.S. Office of Naval Research for their support.

REFERENCES

1. C.S. Clay and H. Medwin, Acoustical Oceanography: Principles and Applications (Wiley-Interscience, New York, 1977). Appendix 10.
2. C. Eckart, "The Scattering of Sound from the Sea Surface," J. Acoust. Soc. Am. 25, 566-570 (1953).
3. S.O. Rice, "Mathematical Analysis of Random Noise," in Selected Papers on Noise and Stochastic Processes, edited by N. Wax (Dover, New York, 1954), pp. 133-294.
4. Herman Medwin, Emily Childs, and Gary M. Jebsen, "Impulse Studies of Double Diffraction: A Discrete Huygens Interpretation," J. Acoust. Soc. Am. 72, 1005-1013 (1982).
5. Wayne A. Kinney, C.S. Clay, and Gerald A. Sandness, "Scattering From a Corrugated Surface: Comparison Between Experiment, Helmholtz-Kirchhoff Theory, and the Facet-Ensemble Method, J. Acoust. Soc. Am. 73, 183-194 (1983).
6. Peter D. Thorne and Nicholas G. Pace, "Acoustic Studies of Broadband Scattering From a Model Rough Surface," J. Acoust. Soc. Am. 75, 133-144 (1984).
7. T.K. Stanton, "Sonar Estimates of Seafloor Microroughness," J. Acoust. Soc. Am. 75, 809-818 (1984).
8. C.S. Clay and W.K. Leong, "Acoustic Estimates of Topography and Roughness Spectrum of the Sea Floor Southwest of Iberian Peninsula," Physics of Sound in Marine Sediments, edited by L. Hampton (Plenum, New York, 1974). This work is summarized in Ref. 1.
9. B.C. Heezen and C.D. Hollister, The Face of the Deep (Oxford U.P., New York, 1971), p. 347.
10. A. David Dunsiger, Norman A. Cochrane, and W.J. Vetter, "Seabed Characterization from Broad-Band Acoustic Echosounding with Scattering Models," IEEE J. Ocean. Eng., OE-6 (3), 94-106 (1981).
11. R.W. Hutchins, D.L. McKeown, and L.H. King, "A Deep Tow High Resolution

Seismic System for Continental Shelf Mapping," Geosci. CANADA, 3, 95-100 (1976)

12. Stanton, T.K., "Echo Fluctuations from the Rough Seafloor: Predictions Based on Acoustically Measured Microrelief Properties," J. Acoust. Soc. Am. (in press).

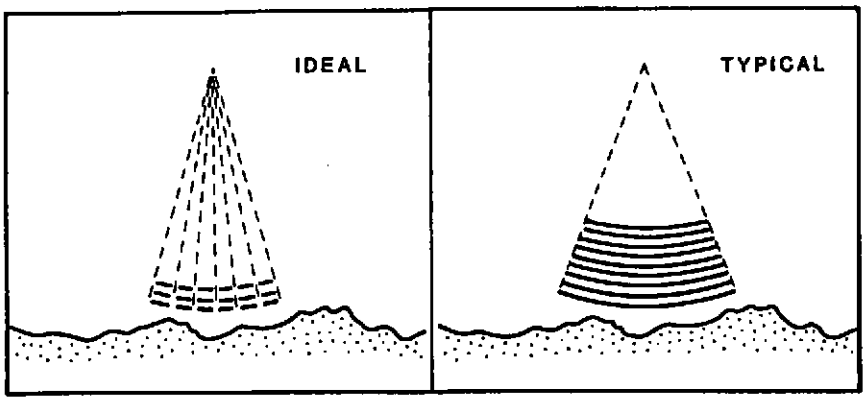

Figure 1. Examples of ideal high resolution sonar (left) and typical low resolution sonar (right).

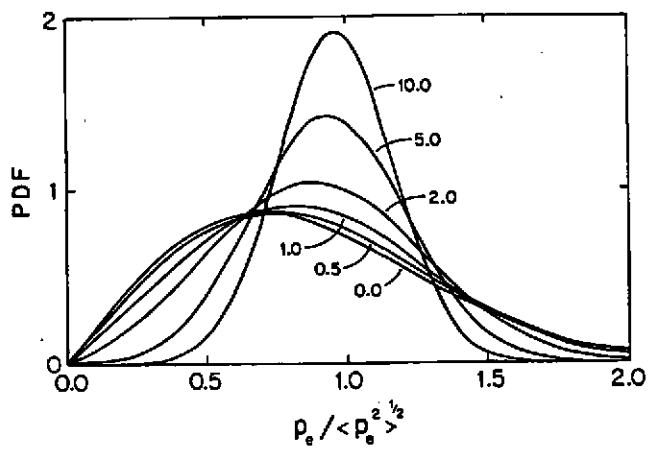

Figure 2. Rice PDF for various values of Y.

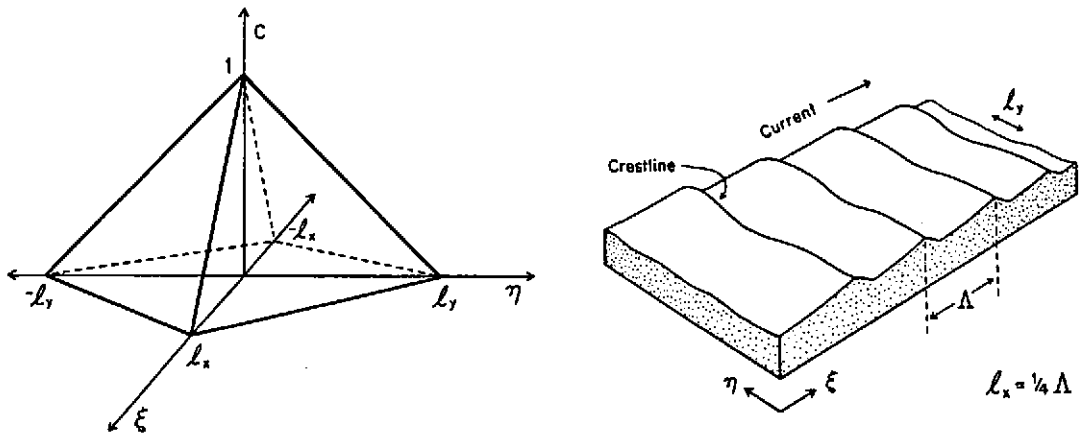

Figure 3. Two-dimensional correlation function of seafloor and typical seafloor where the microrelief is composed of current-generated ripples. From Stanton [7].

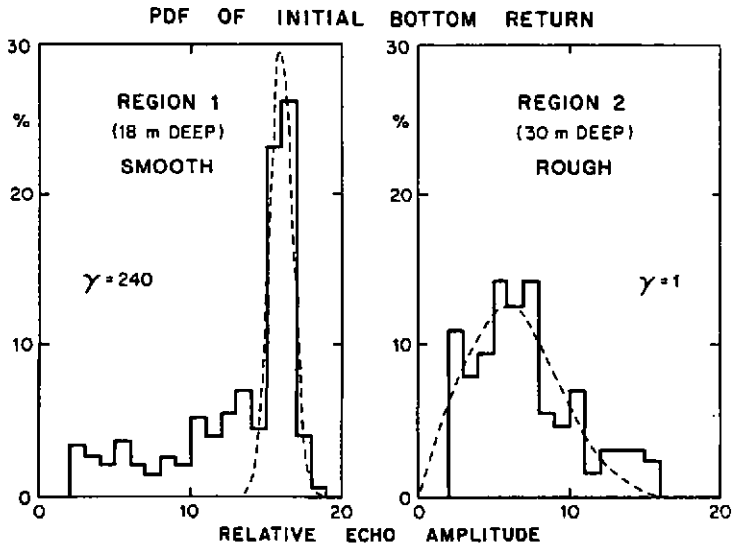

Figure 4. Probability density functions of echo amplitude from a smooth seafloor (Region 1) and rough floor (Region 2). The solid line is data while the dashed is the theoretical Rice PDF. From Stanton [7].

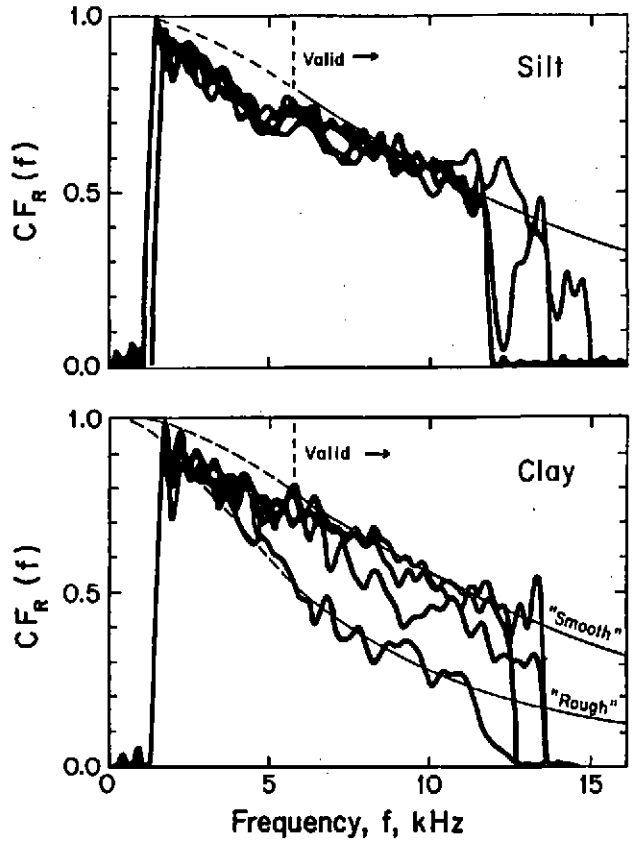

Figure 5. Plots of reflection coherence functions $CF_R(f)$ versus frequency resulting from acoustic data from a downward-looking deep-tow boomer. The data is from clay and silt sediments where the major source of echo fluctuations is due to water/sediment interface microroughness (Redrawn from Dunsiger et al. [10]). The theoretical curves are from Eq. (14) using the form of Υ that was adapted to the boomer measurements in Eq. (15). From Stanton [12].

SEDIMENT TYPE	$\sigma^2 I_C$ (= $\sigma^2 \iint C(\xi,\eta)d\xi d\eta$) (boomer measurement)	σ (photographs)
CLAY	$3.1 - 10 \times 10^{-6} m^4$	0.01 m
SILT	$3.0 \times 10^{-6} m^4$	0.017 m

Figure 6. Listed are values of the important microrelief property of $\sigma^2 I_C$ for clay and silt. The values were extracted from fits of the theoretical curves to the (boomer) measured coherence function in Fig. 5 and will later be used to predict echo amplitude PDFs. From Stanton [12].

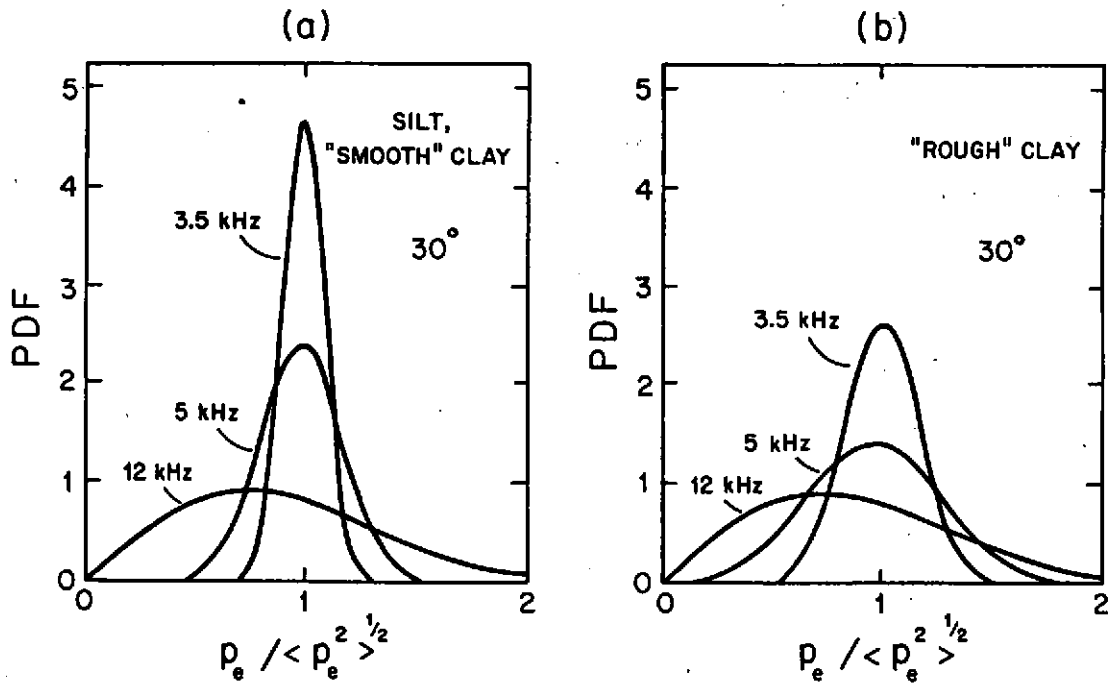

Figure 7. Predictions of echo envelope PDFs for downward looking sonar. The 30° beamwidth given is as measured between the -3dB points. From Stanton [12].

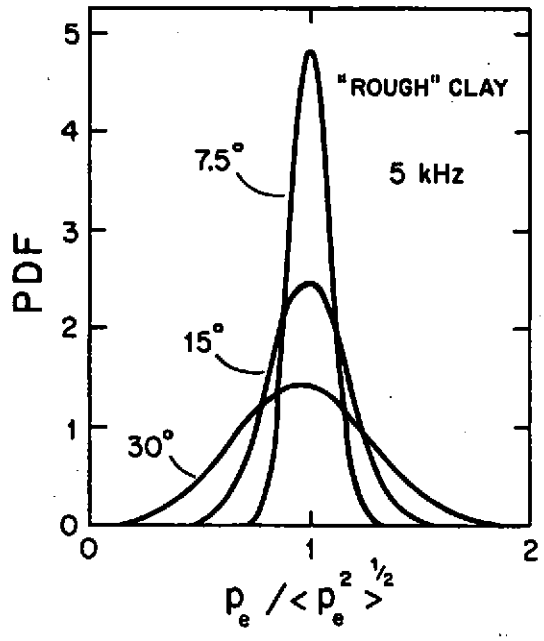

Figure 8. Predictions of echo envelope PDFs for downward looking sonar. The beamwidths given are as measured between the -3dB points. From Stanton [12].